Fairing of discrete planar curves to integrable discrete analogue of Euler's elasticae

Graiff Zurita, Sebastián Elías
Institute of Mathematics for Industry, Kyushu University

Kajiwara, Kenji
Institute of Mathematics for Industry, Kyushu University

Suzuki, Toshitomo
Department of Architecture, Mukogawa Woman's University

出版情報：International Journal of Mathematics for Industry. 14 (01), pp.2250007-1-2250007-20, 2023-03-07. World Scientific Publishing
バージョン：

OPEN ACCESS
International Journal of Mathematics for Industry
Vol. 14, No. 1 (2022) 2250007 (20 pages)

DOI: 10.1142/S2661335222500071

World Scientific
www.worldscientific.com

Fairing of discrete planar curves to integrable discrete analogue of Euler's elasticae

Sebastián Elías Graiff Zurita*,‡, Kenji Kajiwara* and Toshitomo Suzuki†
*Institute of Mathematics for Industry
Kyushu University, 744 Motooka
Nishi-ku, Fukuoka 819-0935, Japan
†Department of Architecture
Mukogawa Woman's University, 1-13 Tozaki-cho
Nishinomiya, Hyogo 663-8121, Japan
‡s-graiff@kyudai.jp

Received 1 November 2021
Revised 2 October 2022
Accepted 8 October 2022
Published 7 March 2023

We construct a method for fairing a given discrete planar curve by using the integrable discrete analog of Euler's elastica, which is a discrete version of the approximation algorithm presented by Brander *et al.* We first give a brief review of the integrable discrete analog of Euler's elastica proposed by Bobenko and Suris, then we present a detailed account of the fairing algorithm, and we apply this method to an architectural problem of characterizing the keylines of Japanese handmade pantiles.

Keywords: Euler's elastica; integrable systems; discrete curve; discrete differential geometry.

1. Introduction

The Euler's elastica (elastic curve) is a class of planar curves characterized as the solutions to the variational problem of minimizing the elastic energy under a certain boundary condition. It has been regarded as one of the most important class of planar curves because it is endowed with rich mathematical structure: exact solutions, integrability, geometry of elliptic curves, and so on, while it serves as a simple but realistic model of thin inextensible elastic rod (see, for example, Refs. 1 and 2). Brander *et al.*[3] have proposed an algorithm for fairing a given planar curve segment by an Euler's elastica, motivated mainly by the development of

‡Corresponding author.

the robotic hot-blade cutting technology. In this work, motivated by a problem of architecture to characterize the keylines of Japanese handmade pantiles, where the curve data are obtained in the form of discrete point data, we aim to construct a fairing method of discrete planar curves by using the integrable discrete analog of the Euler's elastica proposed by Bobenko and Suris,[4] which is referred to as the *discrete elastica* in this paper.

This paper is organized as follows. We give a brief review of the Euler's elastica and the discrete elastica in Secs. 2 and 3, collecting the information on variational formulations, exact solutions and continuum limits with proofs. We present a detailed account of the fairing of a given discrete planar curve to a discrete elastica in Sec. 4. Finally, application to the characterization of the keylines of Japanese handmade pantiles is discussed in Sec. 5. For various formulas of the Jacobi elliptic functions used in this paper, the readers may refer to Ref. 5, for example.

2. Euler's Elastica

Let $\gamma(s) \in \mathbb{R}^2$ ($s \in \mathbb{R}$) be an arc length parameterized planar curve. By definition, it holds that $\|\gamma'(s)\| = 1$, where $' = \frac{d}{ds}$. The tangent and normal vectors are defined by $T(s) = \gamma'(s)$ and $N(s) = R(\pi/2)T(s)$, respectively, where

$$R(\varphi) = \begin{bmatrix} \cos\varphi & -\sin\varphi \\ \sin\varphi & \cos\varphi \end{bmatrix}. \tag{1}$$

Due to $\|\gamma'(s)\| = 1$, it is possible to parameterize the tangent vector as

$$T(s) = \begin{bmatrix} \cos\theta(s) \\ \sin\theta(s) \end{bmatrix}, \tag{2}$$

where the angle function $\theta(s)$ is the angle of $T(s)$ measured from the horizontal axis in the counterclockwise direction. Introducing the Frenet frame $\Phi(s)$ by

$$\Phi(s) = [T(s), N(s)] \in \mathrm{SO}(2), \tag{3}$$

we have the Frenet formula

$$\Phi'(s) = \Phi(s)L(s), \quad L(s) = \begin{bmatrix} 0 & -\kappa(s) \\ \kappa(s) & 0 \end{bmatrix}, \tag{4}$$

where $\kappa(s) = \theta'(s)$ is the (signed) curvature.

The Euler's elastica (or simply referred to as the elastica) is defined as a critical point of the elastic

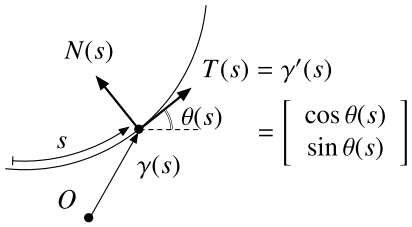

Fig. 1. Smooth planar curve and the Frenet frame.

energy

$$E = \int_0^L (\kappa(s))^2 ds, \tag{5}$$

with respect to variations with fixed endpoints and fixed tangent vectors at the endpoints, under the condition of preserving the total length. The Euler–Lagrange equation yields the following differential equations for the curvature and the angle function.

Proposition 1. *The curvature κ of the Euler's elastica satisfies*

$$\kappa'' + \frac{1}{2}\kappa^3 - \lambda\kappa = 0, \tag{6}$$

where $\lambda \in \mathbb{R}$ is a constant. Moreover, the angle function θ satisfies

$$\theta'' + \mu \sin\theta = 0, \tag{7}$$

where $\mu > 0$ is a constant.

Derivation of Eq. (6) is given in various literatures such as Refs. 2 and 4. Here, we show a concise derivation using the variation of the tangent vector. Consider the functional

$$S = \int_0^L (\langle T', T'\rangle + c\langle T, T\rangle + \langle a, T\rangle) ds, \tag{8}$$

where the first term is the elastic energy, and the second and third terms correspond to the preservation of $\|T\|$ and $\gamma(L) - \gamma(0)$, respectively, with $c = c(s) \in \mathbb{R}$ and $a \in \mathbb{R}^2$ being the Lagrange multipliers. The variation of S is calculated by using the Frenet formula (4) as

$$\begin{aligned} \delta S &= \int_0^L (2\langle T', \delta T'\rangle + 2c(s)\langle T, \delta T\rangle + \langle a, \delta T\rangle) ds \\ &= 2\langle T', \delta T\rangle|_0^L \\ &\quad + 2\int_0^L \left\langle (\kappa^2 + c(s))T - \kappa' N + \frac{a}{2}, \delta T \right\rangle ds. \end{aligned} \tag{9}$$

The first term is the boundary term that vanishes due to the boundary conditions, and the second

term gives the Euler–Lagrange equation

$$(\kappa^2 + c)T - \kappa' N + \frac{a}{2} = 0. \tag{10}$$

Taking the scalar product with T and N, we have

$$\kappa^2 + c + \frac{1}{2}\langle a, T\rangle = 0, \tag{11}$$

$$-\kappa' + \frac{1}{2}\langle a, N\rangle = 0, \tag{12}$$

respectively. Multiplying κ to both sides of Eq. (12), we find that it is integrated to give

$$\frac{\kappa^2}{2} - \lambda = \frac{1}{2}\langle a, T\rangle, \tag{13}$$

where $\lambda \in \mathbb{R}$ is a constant of integration. Eliminating $\langle a, T\rangle$ from Eqs. (11) and (13), c is determined consistently as $c = -\frac{3}{2}\kappa^2 + \lambda$. Differentiating equation (12) gives

$$\kappa'' = -\frac{\kappa}{2}\langle a, T\rangle. \tag{14}$$

Then eliminating $\langle a, T\rangle$ from Eqs. (13) and (14) yields

$$\kappa'' + \kappa\left(\frac{\kappa^2}{2} - \lambda\right) = 0,$$

which is nothing but Eq. (6).

Remark 2.

(1) Equation (6) is derived from Eq. (7) as follows. Multiplying θ' on both sides of Eq. (7), we see that Eq. (7) is integrated to give

$$\frac{1}{2}(\theta')^2 = \mu\cos\theta + \lambda, \tag{15}$$

where λ is a constant of integration. Then differentiating equation (7) and using Eq. (15) yields

$$\kappa'' = -\mu\cos\theta \times \theta' = \left(-\frac{1}{2}\kappa^2 + \lambda\right)\kappa,$$

which is Eq. (6).

(2) Equations (6) and (7) can be seen as traveling-wave reductions of the (focusing) modified Korteweg–de Vries (KdV) equation

$$\frac{\partial\kappa}{\partial t} + \frac{3}{2}\kappa^2\frac{\partial\kappa}{\partial s} + \frac{\partial^3\kappa}{\partial s^3} = 0$$

and the sine-Gordon equation

$$\frac{\partial^2\theta}{\partial s\partial y} = \sin\theta,$$

respectively, where the former describes the integrable deformation of planar curves.[6,7]

It is known that the differential equations (6) and (7) can be solved in terms of the Jacobi elliptic functions. This is well known, but we present the solutions for the readers' convenience. In the literature, the solutions are often constructed from the first integral of (6) given by

$$(\kappa')^2 + \frac{\kappa^4}{2} - \lambda\kappa^2 = C, \tag{16}$$

where C is a conserved quantity (constant). Here, we present those solutions and verify them by the differential equations for the Jacobi elliptic functions.

Proposition 3. *The curvature κ and the angle function θ of an Euler's elastica can be expressed in terms of the Jacobi elliptic functions as follows*:

(i) *Let $\mu = \lambda/(2k^{-2} - 1)$, then*

$$\kappa = 2k^{-1}\sqrt{\mu}\,\mathrm{dn}(k^{-1}\sqrt{\mu}s; k), \tag{17}$$

$$\sin\frac{\theta}{2} = \mathrm{sn}(k^{-1}\sqrt{\mu}s; k). \tag{18}$$

(ii) *Let $\mu = \lambda/(2k^2 - 1)$, then*

$$\kappa = 2k\sqrt{\mu}\,\mathrm{cn}(\sqrt{\mu}s; k), \tag{19}$$

$$\sin\frac{\theta}{2} = k\,\mathrm{sn}(\sqrt{\mu}s; k). \tag{20}$$

Proof. It can be easily verified that Eqs. (17) and (19) satisfy Eq. (6) from the differential equations for the dn and cn functions[5]

$$y = \mathrm{dn}(x, k), \quad \frac{d^2y}{dx^2} = (2 - k^2)y - 2y^3,$$

$$y = \mathrm{cn}(x, k), \quad \frac{d^2y}{dx^2} = (2k^2 - 1)y - 2k^2y^3,$$

respectively, by applying suitable scale transformations. Also, Eqs. (18) and (20) are shown to satisfy Eq. (7) in a similar manner. □

Remark 4. The Jacobi elliptic functions can be extended to modules $k > 1$, see, for example, Refs. 5 and 8. Thus, there exists an analytic continuation for all Jacobi elliptic functions in the range $k \geq 0$. In this way, cases (i) and (ii) can be regarded as one. As it is known, the case (i) (respectively, (ii)) yields the elastica without (respectively, with) inflection points; see Fig. 2.

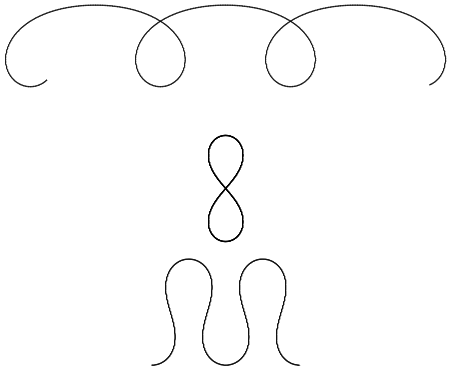

Fig. 2. Typical examples of smooth elasticae. Upper: (i) $k = 0.99$, middle: (ii) $k = 0.9089\ldots$, lower: (ii) $k = 0.8$.

3. Integrable Discrete Euler's Elastica

3.1. *Basic framework of discrete planar curves*

We first introduce the basic framework for discrete planar curves.[9–11] Let $\gamma_n \in \mathbb{R}^2$ $(n \in \mathbb{Z})$ be a discrete planar curve with $|\gamma_{n+1} - \gamma_n| = h$, where $h > 0$ is a constant. We also assume $\det(\gamma_{n+1} - \gamma_n, \gamma_n - \gamma_{n-1}) \neq 0$, i.e., not three consecutive points are collinear. Then γ_n is called a discrete planar curve with segment length h. We define the discrete tangent and normal vectors by

$$T_n = \frac{\gamma_{n+1} - \gamma_n}{h} = \begin{bmatrix} \cos\Theta_n \\ \sin\Theta_n \end{bmatrix}, \tag{21}$$

and $N_n = R(\pi/2)T_n$, respectively, where the discrete angle function Θ_n is the angle of T_n measured from the horizontal axis in the counterclockwise direction. The discrete Frenet frame is defined by

$$\Phi_n = [T_n, N_n] \in \mathrm{SO}(2), \tag{22}$$

and the discrete Frenet formula by

$$\Phi_{n+1} = \Phi_n L_n, \tag{23}$$

where $L_n = R(K_{n+1})$ and $K_n = \Theta_n - \Theta_{n-1}$ is the angle between two adjacent tangent vectors. Equation (23) is the discrete version of the Frenet formula (4); see Fig. 3. The discrete curvature κ_n can be defined as the reciprocal of the radius ρ_n of

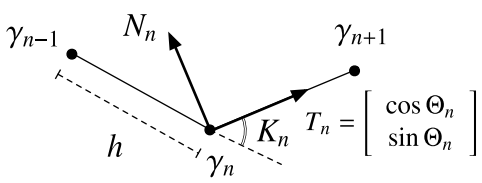

Fig. 3. Discrete planar curve and the Frenet frame.

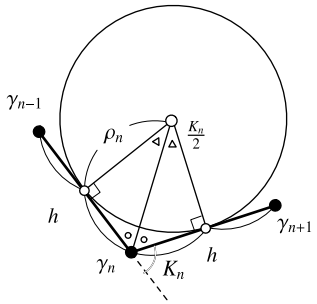

Fig. 4. Discrete curvature of discrete arc length planar curve.

the osculating circle touching two adjacent segments at their midpoints[9] (see Fig. 4)

$$\kappa_n = \frac{1}{\rho_n} = \frac{2}{h}\tan\frac{K_n}{2}. \tag{24}$$

We note that the discrete Frenet formula (23) can be written in terms of κ_n as

$$\frac{\Phi_n - \Phi_{n-1}}{h} = \frac{\Phi_n + \Phi_{n-1}}{2}\begin{bmatrix} 0 & -\kappa_n \\ \kappa_n & 0 \end{bmatrix}. \tag{25}$$

3.2. *Discrete Euler's elastica*

The discrete Euler's elastica[4,12,13] is defined as a critical point of the functional

$$E_d(\gamma) = \sum_{n=1}^{N-1} \frac{2}{h}\log\left(1 + \frac{h^2}{4}\kappa_n^2\right) \tag{26}$$

$$\cong \sum_{n=1}^{N-1} \frac{2}{h}\log(1 + \langle T_{n-1}, T_n\rangle), \tag{27}$$

with respect to variation with fixed endpoints and fixed end edges. Note that $\cong$ means that the two functionals yield the same critical points. As mentioned in Ref. 12, E_d can be regarded as a discrete analog of the elastic energy (5), in a sense that $2/h\log(1 + h^2\kappa_n^2/4)$ is the potential energy of the bending force proportional to the discrete curvature κ_n at each vertex of the discrete curve.

Taking into account the preservation of $\|\gamma_n - \gamma_{n-1}\|$ and $\gamma_N - \gamma_0$ by introducing the Lagrange multipliers $c_n \in \mathbb{R}$ and $a \in \mathbb{R}^2$, respectively, consider the functional

$$S_d = \sum_{n=1}^{N-1} \frac{2}{h}\log(1 + \langle T_{n-1}, T_n\rangle) + \sum_{n=0}^{N-1}(c_n\langle T_n, T_n\rangle + h\langle a, T_n\rangle). \tag{28}$$

Proposition 5. *The Euler–Lagrange equation for the functional* (28) *is given by*

$$\frac{2}{h}\frac{T_{n-1}}{1+\langle T_{n-1},T_n\rangle}+\frac{2}{h}\frac{T_{n+1}}{1+\langle T_n,T_{n+1}\rangle} + 2c_nT_n + ha = 0, \tag{29}$$

or, equivalently, in terms of the discrete curvature κ_n *by*

$$\kappa_{n+1}+\kappa_{n-1} = \frac{\alpha\kappa_n}{1+\frac{h^2}{4}\kappa_n^2}, \tag{30}$$

where $\alpha\in\mathbb{R}$ *is a constant.*

Proof. The variation of S_d is calculated as follows[4,12]:

$$\begin{aligned}\delta S_d &= \sum_{n=1}^{N-1}\left(\frac{2}{h}\frac{\langle\delta T_{n-1},T_n\rangle}{1+\langle T_{n-1},T_n\rangle}+\frac{2}{h}\frac{\langle T_{n-1},\delta T_n\rangle}{1+\langle T_{n-1},T_n\rangle}\right)\\ &\quad+\sum_{n=0}^{N-1}(2c_n\langle T_n,\delta T_n\rangle+h\langle a,\delta T_n\rangle)\\ &= R+\sum_{n=1}^{N-2}\left\langle\frac{2}{h}\frac{T_{n-1}}{1+\langle T_{n-1},T_n\rangle}\right.\\ &\quad\left.+\frac{2}{h}\frac{T_{n+1}}{1+\langle T_n,T_{n+1}\rangle}+2c_nT_n+ha,\delta T_n\right\rangle,\end{aligned}$$

where R is the boundary term given by

$$\begin{aligned}R &= \left\langle\frac{2}{h}\frac{T_1}{1+\langle T_0,T_1\rangle}+2c_0T_0+ha,\delta T_0\right\rangle\\ &\quad+\left\langle\frac{2}{h}\frac{T_{N-2}}{1+\langle T_{N-2},T_{N-1}\rangle}\right.\\ &\quad\left.+2c_{N-1}T_{N-1}+ha,\delta T_{N-1}\right\rangle,\end{aligned}$$

which vanishes due to the boundary condition. Setting $\delta S_d=0$ gives the Euler–Lagrange equation

$$\frac{2}{h}\frac{T_{n-1}}{1+\langle T_{n-1},T_n\rangle}+\frac{2}{h}\frac{T_{n+1}}{1+\langle T_n,T_{n+1}\rangle} + 2c_nT_n + ha = 0, \tag{31}$$

which proves the first part. For the second part we use the discrete Frenet formula (25) written explicitly in terms of the tangent and normal vectors

$$\frac{T_n-T_{n-1}}{h} = \kappa_n\frac{N_n+N_{n-1}}{2}, \tag{32}$$

$$\frac{N_n-N_{n-1}}{h} = -\kappa_n\frac{T_n+T_{n-1}}{2}, \tag{33}$$

we obtain

$$\frac{2}{h}\frac{\langle T_{n-1},N_n\rangle}{1+\langle T_{n-1},T_n\rangle} = -\kappa_n, \tag{34}$$

$$\frac{2}{h}\frac{\langle T_n,N_n\rangle}{1+\langle T_n,T_{n+1}\rangle} = \kappa_{n+1}. \tag{35}$$

Then, taking the inner product of both hand sides of Eq. (31) with N_n, and using Eqs. (34) and (35), gives

$$\kappa_n-\kappa_{n+1} = h\langle a,N_n\rangle. \tag{36}$$

Then, taking the inner product of (32) with a gives

$$\langle a,T_n\rangle-\langle a,T_{n-1}\rangle = -\frac{1}{2}\kappa_n\kappa_{n+1}+\frac{1}{2}\kappa_{n-1}\kappa_n, \tag{37}$$

which implies that exists a constant $\lambda\in\mathbb{R}$ such that

$$\langle a,T_n\rangle = -\frac{1}{2}\kappa_n\kappa_{n+1}+\lambda. \tag{38}$$

Finally taking the inner product of (33) with a, and using Eqs. (36) and (38), yields

$$(\kappa_{n+1}+\kappa_{n-1})\left(1+\frac{h^2}{4}\kappa_n^2\right) = (2+h^2\lambda)\kappa_n, \tag{39}$$

which is exactly Eq. (30) with $\alpha=2+h^2\lambda$. □

By using a technique similar to the one shown in Ref. 14, we construct explicit solutions to Eq. (30) from its discrete first integral,

$$\kappa_{n+1}^2+\kappa_n^2-\alpha\kappa_{n+1}\kappa_n+\frac{h^2}{4}\kappa_{n+1}^2\kappa_n^2 = C, \tag{40}$$

where $C\in\mathbb{R}$ is a constant (conserved quantity). Here, we avoid the long computation required and simply present the solutions corresponding to Eqs. (17) and (19), and verify them by using the addition formulas for the Jacobi elliptic functions.

Proposition 6. *Let* $z,q\in\mathbb{R}$ *be constants. Then the following functions satisfy Eq.* (30).

(i)
$$\begin{aligned}\kappa_n &= \frac{2}{h}\frac{\mathrm{sn}(k^{-1}z;k)}{\mathrm{cn}(k^{-1}z;k)}\mathrm{dn}(k^{-1}(zn+q);k),\\ \alpha &= 2\frac{\mathrm{dn}(k^{-1}z;k)}{\mathrm{cn}^2(k^{-1}z;k)}.\end{aligned} \tag{41}$$

(ii)
$$\begin{aligned}\kappa_n &= \frac{2}{h}\frac{k\mathrm{sn}(z;k)}{\mathrm{dn}(z;k)}\mathrm{cn}(z(n+q);k),\\ \alpha &= 2\frac{\mathrm{cn}(z;k)}{\mathrm{dn}^2(z;k)}.\end{aligned} \tag{42}$$

Proof. These solutions are verified directly by the addition formulas for the dn and cn functions.[5] On the one hand, we use that

$$\mathrm{dn}(u+v)+\mathrm{dn}(u-v)=\frac{\frac{2\mathrm{dn}v}{\mathrm{cn}^2v}\mathrm{dn}u}{1+\frac{\mathrm{sn}^2v}{\mathrm{cn}^2v}\mathrm{dn}^2u}. \tag{43}$$

Putting $u=k^{-1}(zn+q)$, $v=k^{-1}z$, and $\kappa_n=a\mathrm{dn}(u;k)$, and comparing Eq. (43) with Eq. (30), we see that

$$\frac{1}{a^2}\frac{\mathrm{sn}^2v}{\mathrm{cn}^2v}=\frac{h^2}{4},\qquad \frac{2\mathrm{dn}v}{\mathrm{cn}^2v}=\alpha,$$

which proves (i). Similarly, on the other hand we use

$$\mathrm{cn}(u+v)+\mathrm{cn}(u-v)=\frac{\frac{2\mathrm{cn}v}{\mathrm{dn}^2v}\mathrm{cn}u}{1+\frac{k^2\mathrm{sn}^2v}{\mathrm{dn}^2v}\mathrm{cn}^2u}. \tag{44}$$

Then putting $u=zn+q$, $v=z$, and $\kappa_n=b\mathrm{cn}(u;k)$, we get Eq. (30) with

$$\frac{1}{b^2}\frac{k^2\mathrm{sn}^2v}{\mathrm{dn}^2v}=\frac{h^2}{4},\quad \frac{2\mathrm{cn}v}{\mathrm{dn}^2v}=\alpha,$$

which proves (ii). □

Remark 7

(1) Comparing Eqs. (17) and (41), we see that there exists constants $\Omega, s_0\in\mathbb{R}$ such that $\kappa_n=\kappa(\Omega n+s_0)$. Indeed, we have

$$\Omega=\frac{z}{\sqrt{\mu}},\quad s_0=\frac{q}{\sqrt{\mu}}, \tag{45}$$

with

$$\mu=\frac{k^2h^{-2}}{(\mathrm{sn}(z;k))^{-2}-1}. \tag{46}$$

There is also a similar relationship between Eqs. (19) and (42). This implies that the discrete curvature κ_n is an "exact discretization" of the smooth curvature $\kappa(s)$.

(2) By putting $\alpha=h^2\lambda+2$ and $nh=s$, Eq. (30) yields Eq. (6) in the continuum limit $h\to 0$. On the level of solutions, the following parametrizations of z

$$z=\begin{cases}\sqrt{\dfrac{\lambda}{2k^{-2}-1}}\,h & \text{for (i)},\quad (47)\\[2ex] \sqrt{\dfrac{\lambda}{2k^{2}-1}}\,h & \text{for (ii)},\quad (48)\end{cases}$$

are consistent in the continuum limit to Eqs. (18) and (20), respectively.

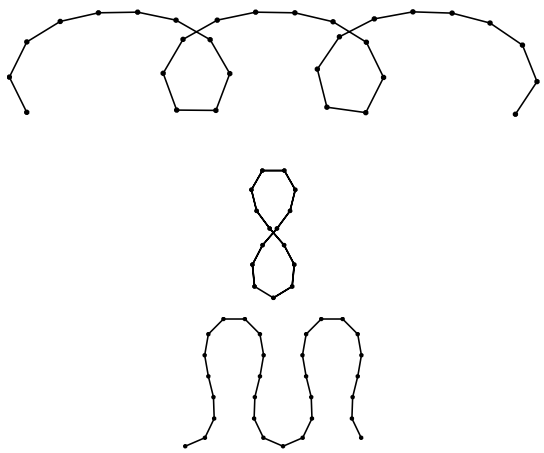

Fig. 5. Typical examples of discrete elasticae. Upper: (i) $k=0.99$, middle: (ii) $k=0.919\ldots$, lower: (ii) $k=0.8$.

(3) Equation (30) is also known as the McMillan map, which is a special case of the Quispel–Roberts–Thompson (QRT) map solved by elliptic functions.[15] It can also be regarded as an autonomous version of a discrete Painlevé II equation.[16–18]

(4) It is known that position vectors of both smooth and discrete elasticae admit explicit formulas in terms of the elliptic theta functions.[19,20]

Figure 5 illustrates typical examples of discrete elasticae.

3.3. *Discrete Euler's elastica in terms of a potential function*

Following Ref. 7, we say that θ_n is a *potential function* if it is such that

$$\Theta_n=\frac{\theta_{n+1}+\theta_n}{2}. \tag{49}$$

In this context, the discrete curvature is written as

$$\kappa_n=\frac{2}{h}\tan\left(\frac{\theta_{n+1}-\theta_{n-1}}{4}\right). \tag{50}$$

Proposition 8. *Suppose that θ_n satisfies*

$$\sin\left(\frac{\theta_{n+1}-2\theta_n+\theta_{n-1}}{4}\right)+\epsilon\sin\left(\frac{\theta_{n+1}+2\theta_n+\theta_{n-1}}{4}\right)=0, \tag{51}$$

where $\epsilon > 0$ is a constant. Then we have

(1) *It holds that*

$$\cos\left(\frac{\theta_{n+1}-\theta_n}{2}\right)+\epsilon\cos\left(\frac{\theta_{n+1}+\theta_n}{2}\right)=\Lambda, \tag{52}$$

where $\Lambda \in \mathbb{R}$ is a constant.

(2) *The discrete curvature satisfies Eq. (30) with $\alpha = 2(1-\epsilon^2)/\Lambda^2$.*

Proof. The first statement is shown as follows. Multiplying $\sin(\frac{\theta_{n+1}-\theta_{n-1}}{4})$ to Eq. (51), using the product-to-sum formula, and rearranging terms gives:

$$\begin{aligned}&\cos\left(\frac{\theta_{n+1}-\theta_n}{2}\right)+\epsilon\cos\left(\frac{\theta_{n+1}+\theta_n}{2}\right)\\&\quad=\cos\left(\frac{\theta_n-\theta_{n-1}}{2}\right)+\epsilon\cos\left(\frac{\theta_n+\theta_{n-1}}{2}\right),\end{aligned}$$

which implies (52). In order to show the second statement, we introduce

$$\varphi_n=\frac{\theta_{n+1}-\theta_n}{2},\quad \psi_n=\frac{\theta_{n+1}+\theta_n}{2}, \tag{53}$$

for simplicity in the notation. We have that $K_n=\psi_n-\psi_{n-1}=\varphi_n+\varphi_{n-1}$, and Eq. (51) is rewritten as

$$\sin\left(\frac{\varphi_n-\varphi_{n-1}}{2}\right)=-\epsilon\sin\left(\frac{\psi_n+\psi_{n-1}}{2}\right). \tag{54}$$

We expand Eq. (54) as

$$\begin{aligned}&\sin\varphi_n\cos\frac{K_n}{2}-\cos\varphi_n\sin\frac{K_n}{2}\\&\quad=-\epsilon\sin\psi_n\cos\frac{K_n}{2}+\epsilon\cos\psi_n\sin\frac{K_n}{2},\end{aligned}$$

which gives

$$\tan\frac{K_n}{2}=\frac{\sin\varphi_n+\epsilon\sin\psi_n}{\Lambda}, \tag{55}$$

$$\tan\frac{K_{n+1}}{2}=\frac{\sin\varphi_n-\epsilon\sin\psi_n}{\Lambda}, \tag{56}$$

where we used Eq. (52). From Eqs. (55) and (56), and the sum-to-product formula, we have

$$\begin{aligned}&\Lambda\left(\tan\frac{K_{n+1}}{2}+\tan\frac{K_{n-1}}{2}\right)\\&\quad=2\sin\frac{K_n}{2}\left[\cos\left(\frac{\varphi_n-\varphi_{n-1}}{2}\right)-\epsilon\cos\left(\frac{\psi_n+\psi_{n-1}}{2}\right)\right].\end{aligned} \tag{57}$$

We use the following two expressions: On the one hand, from Eq. (51)

$$\cos^2\left(\frac{\varphi_n-\varphi_{n-1}}{2}\right)-\epsilon^2\cos^2\left(\frac{\psi_n+\psi_{n-1}}{2}\right)=1-\epsilon^2. \tag{58}$$

On the other hand,

$$\begin{aligned}&\cos\left(\frac{\varphi_n-\varphi_{n-1}}{2}\right)+\epsilon\cos\left(\frac{\psi_n+\psi_{n-1}}{2}\right)\\&\quad=\cos\frac{K_n}{2}\left(\cos\varphi_n+\epsilon\cos\psi_n\right)\\&\qquad+\sin\frac{K_n}{2}\left(\sin\varphi_n+\epsilon\sin\psi_n\right)\\&\quad=\frac{\Lambda}{\cos\frac{K_n}{2}},\end{aligned} \tag{59}$$

where we used Eqs. (52) and (55). Finally, we multiply Eq. (57) by Eq. (59) to obtain

$$\Lambda\left(\tan\frac{K_{n+1}}{2}+\tan\frac{K_{n-1}}{2}\right)\frac{\Lambda}{\cos\frac{K_n}{2}}=2\sin\frac{K_n}{2}(1-\epsilon^2),$$

where we used (58), which is rewritten as

$$\tan\frac{K_{n+1}}{2}+\tan\frac{K_{n-1}}{2}=\frac{1-\epsilon^2}{\Lambda^2}\,\frac{2\tan\frac{K_n}{2}}{1+\tan^2\frac{K_n}{2}}. \tag{60}$$

From the definition of discrete curvature, Eq. (60) is equivalent to Eq. (30) with $\alpha = 2(1-\epsilon^2)/\Lambda^2$, which proves the second statement. □

Remark 9. Proposition 8 provides discrete analogs for Eqs. (7) and (15). In fact, by putting

$$\Lambda=1-\frac{h^2}{4}\lambda,\quad \epsilon=\frac{h^2}{4}\mu,\quad s=nh, \tag{61}$$

Equations (51) and (52) yield Eqs. (7) and (15) in the continuum limit $h \to 0$.

We next present explicit solutions for Eq. (51). Part of Propositions 10 and 12 can be found in Ref. 21, in a slightly different context: in that work, the function θ_n is regarded as the angle function (here denoted as Θ_n) instead of a potential function.

Proposition 10. *The following functions satisfy Eq. (51):*

(i)

$$\begin{aligned}\sin\frac{\theta_n}{2}&=\mathrm{sn}(k^{-1}(zn+q);k),\\ \mathrm{dn}(k^{-1}z;k)&=\frac{1-\epsilon}{1+\epsilon}.\end{aligned} \tag{62}$$

(ii)

$$\begin{aligned} \sin\frac{\theta_n}{2} &= k\mathrm{sn}(zn+q;k), \\ \mathrm{cn}(z;k) &= \frac{1-\epsilon}{1+\epsilon}. \end{aligned} \tag{63}$$

Proof. For convenience, we write $u = k^{-1}(zn+q)$ and $v = k^{-1}z$. For (i), we show that Eq. (62) satisfies Eq. (52). Note that $\cos(\theta_n/2) = \mathrm{cn}u$ and $\cos(\theta_{n+1}/2) = \mathrm{cn}(u+v)$. Then, the right-hand side of Eq. (52) is rewritten as

$$\begin{aligned} &\cos\left(\frac{\theta_{n+1}-\theta_n}{2}\right) + \epsilon\cos\left(\frac{\theta_{n+1}+\theta_n}{2}\right) \\ &\quad = \frac{1}{1-k^2\mathrm{sn}^2u\mathrm{sn}^2v}[\{(1+\epsilon)\mathrm{cn}^2u \\ &\qquad + (1-\epsilon)\mathrm{sn}^2u\mathrm{dn}v\}\mathrm{cn}v + \{-(1+\epsilon)\mathrm{dn}v \\ &\qquad + (1+\epsilon)\}\mathrm{sn}\,u\mathrm{sn}\,v\mathrm{cn}\,u\mathrm{dn}v], \end{aligned} \tag{64}$$

where we used the addition formulas for the cn and sn functions. Imposing $\mathrm{dn}v = (1+\epsilon)/(1-\epsilon)$, we see that Eq. (52) is consistently reduced to $\Lambda = (1+\epsilon)\mathrm{cn}v$. We prove (ii) in a similar manner. In fact, noticing that $\cos(\theta_n/2) = \mathrm{dn}u$ and imposing $\mathrm{cn}v = (1+\epsilon)(1-\epsilon)$, Eq. (52), with $u = zn+q$ and $v = z$, is consistently reduced to $\Lambda = (1+\epsilon)\mathrm{dn}v$. □

Remark 11

(1) In case (i), the parameter α in Eq. (30) is given by

$$\alpha = 2\frac{(1-\epsilon^2)}{\Lambda^2} = 2\frac{\mathrm{dn}(k^{-1}z;k)}{\mathrm{cn}^2(k^{-1}z;k)}, \tag{65}$$

which implies that θ_n in Eq. (62) corresponds to κ_n in Eq. (41). In case (ii),

$$\alpha = 2\frac{(1-\epsilon^2)}{\Lambda^2} = 2\frac{\mathrm{cn}(z;k)}{\mathrm{dn}^2(z;k)}, \tag{66}$$

so that θ_n in Eq. (63) corresponds to κ_n in Eq. (42). These correspondences can be verified directly by computing κ_n from Eqs. (62) and (63), respectively.

(2) Continuum limits of Eqs. (62) and (63) to Eqs. (41) and (42), respectively, are obtained by putting $\epsilon = \frac{\mu}{4}h^2$ and taking the limit of $h \to 0$. This is consistent with Remark 7.

We finally present the variational formulation for Eq. (51).

Proposition 12 (Ref. 21, Sec. 2). *Equation* (51) *is equivalent to the Euler–Lagrange equation of the functional*

$$\tilde{S}_d = \sum_{n=0}^{N-1}\cos\left(\frac{\theta_{n+1}-\theta_n}{2}\right) - \epsilon\cos\left(\frac{\theta_{n+1}+\theta_n}{2}\right),$$

with respect to variations of the potential angle θ_n *with fixed endpoints.*

Proof. Let

$$L(\theta_n,\theta_{n+1}) = \cos\left(\frac{\theta_{n+1}-\theta_n}{2}\right) - \epsilon\cos\left(\frac{\theta_{n+1}+\theta_n}{2}\right).$$

Then, the Euler–Lagrange equation is calculated as

$$\begin{aligned} 0 &= \frac{\partial}{\partial\theta_n}L(\theta_n,\theta_{n+1}) + \frac{\partial}{\partial\theta_n}L(\theta_{n-1},\theta_n) \\ &= \cos\left(\frac{\theta_{n+1}-\theta_{n-1}}{4}\right)\left[\sin\left(\frac{\theta_{n+1}-2\theta_n+\theta_{n-1}}{4}\right)\right. \\ &\quad \left. + \epsilon\sin\left(\frac{\theta_{n+1}+2\theta_n+\theta_{n-1}}{4}\right)\right], \end{aligned}$$

which gives Eq. (51). □

Remark 13. Equation (51) can be seen as a reduction of two well-known equations:

(1) The discrete sine-Gordon equation[10,22,23]

$$\begin{aligned} &\sin\left(\frac{\theta_{l+1}^{m+1}-\theta_l^{m+1}-\theta_{l+1}^m+\theta_l^m}{4}\right) \\ &\quad = \frac{a}{b}\sin\left(\frac{\theta_{l+1}^{m+1}+\theta_l^{m+1}+\theta_{l+1}^m+\theta_l^m}{4}\right), \end{aligned}$$

where a, b are lattice intervals. In fact, assuming that θ depends only on $n = l+m$, this equation is reduced to Eq. (51) with $\epsilon = -\frac{b}{a}$.

(2) The discrete potential modified KdV equation[24]

$$\tan\frac{\theta_{l+1}^{m+1}-\theta_l^m}{4} = \frac{b+a}{b-a}\tan\frac{\theta_l^{m+1}-\theta_{l+1}^m}{4},$$

or equivalently

$$\begin{aligned} &\sin\left(\frac{\theta_{l+1}^{m+1}-\theta_l^{m+1}+\theta_{l+1}^m-\theta_l^m}{4}\right) \\ &\quad = \frac{a}{b}\sin\left(\frac{\theta_{l+1}^{m+1}+\theta_l^{m+1}-\theta_{l+1}^m-\theta_l^m}{4}\right), \end{aligned}$$

which describes the isoperimetric and equidistant deformation of discrete planar curves,[7,11] is transformed to the discrete sine-Gordon equation by $\theta_l^m \to (-1)^m\theta_l^m$. In this sense, Eq. (51) can

also be regarded as a reduction of the discrete potential modified KdV equation.

4. Approximation of Discrete Curves

In this section, we construct an algorithm to approximate a given discrete planar curve to a discrete elastica. Among the many possible discretizations for the elastica, the advantages of using the one shown in this work can be described as follows: First, the discrete elasticae are endowed with the same integrable structure as in their smooth counterpart, i.e., they possess several conserved quantities, can be obtained via a variational principle, and their explicit solutions are expressed in terms of Jacobi elliptic functions. Moreover, it is known that variational integrators have controlled error in their solutions.[25–27] In particular, the explicit expression for the discrete curvature κ_n is an "exact discretization" of the smooth curvature $\kappa(s)$ as discussed in Remark 7, and the potential function θ_n has the same functional shape as the smooth angle function $\theta(s)$. From these observations, we expect this discretization to have good numerical properties.

4.1. *General discrete Euler's elastica segment*

To describe a general curve segment in the plane, we include the freedom of rotation in the equations. We do this by shifting the angle function and discrete angle function by a constant $\phi \in \mathbb{R}$ in all the expressions. In particular, Eq. (51) goes to

$$\sin\left(\frac{\theta_{n+1}-2\theta_n+\theta_{n-1}}{4}\right) + \frac{\mu h^2}{4}\sin\left(\frac{\theta_{n+1}+2\theta_n+\theta_{n-1}}{4}-\phi\right)=0, \tag{67}$$

where we put $\epsilon = \mu h^2/4$, with $\mu > 0$ a constant. From Proposition 10, we have

(i)

$$\begin{aligned}\cos\frac{\theta_n-\phi}{2} &= \mathrm{cn}(k^{-1}(zn+q);k),\\ \sin\frac{\theta_n-\phi}{2} &= \mathrm{sn}(k^{-1}(zn+q);k),\end{aligned} \tag{68}$$

(ii)

$$\begin{aligned}\cos\frac{\theta_n-\phi}{2} &= \mathrm{dn}(zn+q;k),\\ \sin\frac{\theta_n-\phi}{2} &= k\,\mathrm{sn}(zn+q;k),\end{aligned} \tag{69}$$

where $k > 0$, $q, z \in \mathbb{R}$ are constants. The parameter k determines the shape of the elastica, q the initial point, and z is related with the length and point aggregation of the curve segment. From its starting point $\gamma_0 \in \mathbb{R}^2$, a discrete elastica segment is calculated recursively by

$$\gamma_n = \gamma_{n-1} + h\begin{bmatrix}\cos\left(\frac{\theta_{n+1}-\phi}{2}+\frac{\theta_n-\phi}{2}-\phi\right)\\ \sin\left(\frac{\theta_{n+1}-\phi}{2}+\frac{\theta_n-\phi}{2}-\phi\right)\end{bmatrix}, \tag{70}$$

for all $n = 1, \ldots, N-1$. Note that we can expand the sine and cosine in Eq. (70) and make use of Eqs. (68) and (69) to obtain an explicit expression in terms of the Jacobi elliptic functions. We use the analytic continuation of the Jacobi elliptic functions and extend the domain of the module to $k > 0$. Finally, we conclude that a general discrete elastica segment can be characterized by the seven parameters

$$p = (x_0, y_0, h, \phi, z, q, k), \tag{71}$$

where $x_0, y_0 \in \mathbb{R}$ are the two components of the initial point γ_0. We write as $\gamma_n(p)$ to the discrete elastica with parameters p.

4.2. *Fairing process*

Given a general discrete curve segment $\zeta_n \in \mathbb{R}^2$ $(n = 0, \ldots, N-1)$, we look for a discrete elastica $\gamma_n(p) \in \mathbb{R}^2$ that is the closest, in a L^2-distance sense, to ζ_n. Namely, we seek to find p^* such that

$$p^* = \underset{p\in U}{\mathrm{argmin}}\left\{\sum_{n=0}^{N-1}\frac{1}{2}\|\gamma_n(p)-\zeta_n\|^2\right\}, \tag{72}$$

where

$$U = \{(x_0, y_0, h, \phi, z, q, k)| \; x_0, y_0, z, q \in \mathbb{R} \wedge \phi \in [0, 2\pi) \wedge h, k > 0\}.$$

We solve this non-convex problem using the Interior Point Optimizer (IPOPT) package, that for our purpose can be seen as a gradient descent-like

method for nonlinear optimizations.[28] For its implementation we need to compute the gradient and the Hessian of the objective function

$$\mathcal{L}(p) := \sum_{n=0}^{N-1} \frac{1}{2} \|\gamma_n(p) - \zeta_n\|^2. \tag{73}$$

For the gradient, we have

$$\frac{\partial}{\partial p_i}\mathcal{L}(p) = \sum_{n=0}^{N-1} \left\langle \gamma_n(p) - \zeta_n, \frac{\partial}{\partial p_i}\gamma_n(p) \right\rangle, \tag{74}$$

with $p_i = x_0, y_0, h, \phi, z, q, k$, which is computed recursively from Eq. (70) by

$$\frac{\partial}{\partial p_i}\gamma_n(p) = \frac{\partial}{\partial p_i}\gamma_{n-1}(p) + \begin{cases} 0, & p_i = x_0, y_0, \\ T_n, & p_i = h, \\ h\dfrac{\partial}{\partial p_i}T_n & \text{otherwise}, \end{cases}$$

and

$$\frac{\partial}{\partial p_i}\gamma_0 = \begin{cases} \begin{pmatrix} 1 \\ 0 \end{pmatrix}, & p_i = x_0, \\ \begin{pmatrix} 0 \\ 1 \end{pmatrix}, & p_i = y_0, \\ \begin{pmatrix} 0 \\ 0 \end{pmatrix} & \text{otherwise}. \end{cases}$$

Then, the only nontrivial derivatives we need to compute are

$$\frac{\partial}{\partial p_i}T_n = N_n\left(\frac{1}{C_{n+1}(p)}\frac{\partial}{\partial p_i}S_{n+1}(p) + \frac{1}{C_n(p)}\frac{\partial}{\partial p_i}S_n(p)\right),$$

or equivalently,

$$\frac{\partial}{\partial p_i}T_n = -N_n\left(\frac{1}{S_{n+1}(p)}\frac{\partial}{\partial p_i}C_{n+1}(p) + \frac{1}{S_n(p)}\frac{\partial}{\partial p_i}C_n(p)\right),$$

for $p_i = z, q, k$, where we denoted $S_n \equiv \sin\frac{\theta_n - \phi}{2}$ and $C_n \equiv \cos\frac{\theta_n - \phi}{2}$. Finally, we use Eqs. (68), (69) and the derivatives of the Jacobi elliptic functions with respect to their argument and module to complete the computation. For the Hessian, we use a numerical quasi-Newton approximation, internally computed by the package.

The IPOPT method needs a starting point $\hat{p}$, that we refer as the *initial guess*. In the following section, we describe the algorithm that we use to obtain the initial guess, which is a discrete analog of the one provided in Ref. 3.

4.3. *Initial parameters*

The initial guess, that starts the IPOPT method, can be obtained in a numerically stable manner thanks to two geometric properties of the discrete elastica: Proposition 14 and Corollary 14. Remarkably, these are geometrically equivalent to the same properties for the smooth elastica.[3] Let

$$\mathrm{I} = \begin{bmatrix} \sin\phi \\ -\cos\phi \end{bmatrix} \in \mathbb{R}^2,$$

and define the projection of the curve γ_n onto I as

$$u_n = \langle \mathrm{I}, \gamma_n \rangle, \tag{75}$$

and the angle measured from I as $\Psi_n = \frac{\pi}{2} + \Theta_n - \phi$, which satisfies that

$$\begin{cases} \cos\Psi_n = -\sin(\Theta_n - \phi), \\ \sin\Psi_n = \cos(\Theta_n - \phi). \end{cases} \tag{76}$$

Proposition 14. *The discrete curvature κ_n is an affine function of the projection u_n, satisfying*

$$\kappa_n = \frac{\mu}{\Lambda}u_n + A, \tag{77}$$

where $\Lambda \in \mathbb{R}$ satisfies Eq. (52) and $A \in \mathbb{R}$ is a constant.

Proof. In the context of the proof of Proposition 8, after incorporating ϕ and putting $\epsilon = \mu h^2/4$, from Eqs. (55) and (56) we obtain

$$\frac{\kappa_{n+1} - \kappa_n}{h} = -\frac{\mu}{\Lambda}\sin(\Theta_n - \phi). \tag{78}$$

Then, noticing that $u_{n+1} - u_n = h\langle I, T_n\rangle$, we have

$$\frac{u_{n+1} - u_n}{h} = -\sin(\Theta_n - \phi). \tag{79}$$

Hence, by comparing Eqs. (77) and (78), we conclude that there exists a constant $A \in \mathbb{R}$ such that, for all n,

$$\kappa_n = \frac{\mu}{\Lambda}u_n + A. \tag{80}$$

□

Note that, by putting $\mu_1 = \mu\cos\phi$ and $\mu_2 = \mu\sin\phi$, Eq. (77) can be expressed as

$$\kappa_n = \frac{1}{\Lambda}(\mu_2 x_n - \mu_1 y_n) + A, \tag{81}$$

where $x_n, y_n \in \mathbb{R}$ are the two components of γ_n.

Corollary 15. *It holds that*

$$\sin\Psi_n = \frac{\mu}{2\Lambda}u_{n+1}u_n + A\frac{u_{n+1}+u_n}{2} + B, \tag{82}$$

where $B \in \mathbb{R}$ is a constant.

Proof. From the definition of u_n and Ψ_n in Eqs. (75) and (76), respectively, we obtain

$$T_n = R(\phi)\begin{bmatrix}\sin\Psi_n \\ -\frac{u_{n+1}-u_n}{h}\end{bmatrix},$$

and

$$N_n = R(\phi)\begin{bmatrix}\frac{u_{n+1}-u_n}{h} \\ \sin\Psi_n\end{bmatrix}.$$

Then, putting this into the Frenet formula $(T_n - T_{n-1})/h = \kappa_n(N_n + N_{n-1})/2$ gives

$$\sin\Psi_n - \sin\Psi_{n-1} = \frac{1}{2}\left(\frac{\mu}{\Lambda}u_n + A\right)(u_{n+1} - u_{n-1}),$$

where we used (77). After expanding the right-hand side of the previous expression and then adding $\pm\frac{A}{2}u_n$, we conclude that there exists a constant $B \in \mathbb{R}$ such that, for all n,

$$\sin\Psi_n = \frac{\mu}{2\Lambda}u_{n+1}u_n + A\frac{u_{n+1}+u_n}{2} + B. \tag{83}$$

□

To estimate (ϕ, z, q, k) we use some results from the smooth elastica to avoid unnecessary complexity in the discrete case. We use the following approximations: From Eq. (52) with $\epsilon = \mu h^2/4$, taking Eq. (61) into account, Eqs. (81) and (82) can be expanded in terms of $\sqrt{\mu}h$ as

$$\kappa_n = \mu_2 x_n - \mu_1 y_n + A + \mathcal{O}(\mu h^2), \tag{84}$$

and

$$\sin\Psi_n = \frac{1}{2}\mu u_n^2 + Au_n + B + \mathcal{O}(\mu h^2), \tag{85}$$

respectively. For the discrete curvature, note that solutions (41) and (42) can be written, respectively, as

(i) Let $\kappa_{\max} = \frac{2}{h}\frac{\mathrm{sn}(k^{-1}z;k)}{\mathrm{cn}(k^{-1}z;k)}$, then

$$\kappa_n = \kappa_{\max}\mathrm{dn}(k^{-1}(zn+q);k). \tag{86}$$

(ii) Let $\kappa_{\max} = \frac{2}{h}\frac{k\mathrm{sn}(z;k)}{\mathrm{dn}(z;k)}$, then

$$\kappa_n = \kappa_{\max}\mathrm{cn}(zn+q;k). \tag{87}$$

From Remark 11, we have $\alpha = 2 + \lambda h^2 + \mathcal{O}(h^4)$, and it follows from Eqs. (47) and (48) that $z = \sqrt{\mu}h + \mathcal{O}(h^2)$. Then we can approximate $\kappa_{\max}$ as

$$\begin{cases}\text{(i)}: & \kappa_{\max} = 2k^{-1}\sqrt{\mu} + \mathcal{O}(\mu h^2), \\ \text{(ii)}: & \kappa_{\max} = 2k\sqrt{\mu} + \mathcal{O}(\mu h^2).\end{cases} \tag{88}$$

We obtain an approximation of the parameter k from these expressions. We see from Eq. (85) that u must be bound from above and below, the upper bound $u_{\max}$ being

$$u_{\max} = \frac{-A+\Delta}{\mu} + \mathcal{O}(h^2), \tag{89}$$

where $\Delta = \sqrt{A^2 - 2\mu(B-1)}$. Noticing that $u_{\max}$ occurs at the same instance as $\kappa_{\max}$, from Eq. (77) we have

$$\kappa_{\max} = \Delta + \mathcal{O}(\mu h^2). \tag{90}$$

Hence, from Eq. (88) we obtain

$$\begin{cases}\text{(i)}: & k = \dfrac{2\sqrt{\mu}}{\Delta} + \mathcal{O}(\sqrt{\mu}h^2), \\ \text{(ii)}: & k = \dfrac{\Delta}{2\sqrt{\mu}} + \mathcal{O}(\sqrt{\mu}h^2).\end{cases} \tag{91}$$

Pseudo code

Given a discrete curve ζ_n $(n = 0, 1, \ldots, N-1)$ with segment length h, we compute Θ_n such that

$$\begin{bmatrix}\cos\Theta_n \\ \sin\Theta_n\end{bmatrix} = \frac{\zeta_{n+1} - \zeta_n}{h}, \tag{92}$$

for all $n = 0, 1, \ldots, N-2$, and the discrete curvature κ_n by

$$\kappa_n := \frac{2}{h}\tan\frac{\Theta_n - \Theta_{n-1}}{2}, \tag{93}$$

for all $n = 1, 2, \ldots, N-2$. Then, we obtain the initial guess $\hat{p}$ by solving Eqs. (84) and (85) in the least-square sense and using several of the equations mentioned above. We proceed as follows:

- (parameter ϕ) From Eq. (84), compute

$$(\hat{\mu}_1, \hat{\mu}_2, \hat{\mathrm{A}}) = \underset{(\mu_1,\mu_2,A)}{\mathrm{argmin}}\left\{\sum_{n=1}^{N-2}(\kappa_n + \mu_1 y_n - \mu_2 x_n - A)^2\right\},$$

then $\hat{\mu} = \sqrt{\hat{\mu}_1^2 + \hat{\mu}_2^2}$, and ϕ is such that $\cos\phi = \hat{\mu}_1/\hat{\mu}$ and $\sin\phi = \hat{\mu}_2/\hat{\mu}$.

- (parameter k) From Eq. (85), compute

$$\hat{B} = \underset{B}{\operatorname{argmin}} \left\{ \sum_{n=0}^{N-2} \left(\sin \Psi_n - \frac{1}{2}\hat{\mu} u_n^2 - \hat{\mathrm{A}} u_n - B \right)^2 \right\}.$$

From Eq. (91), if $\hat{B} < \frac{\hat{\mathrm{A}}^2}{2\hat{\mu}} - 1$, then we are in case (i) and

$$\text{(i)}: \quad \hat{k} = 2\left(\frac{\hat{\mathrm{A}}^2}{\hat{\mu}} - 2(\hat{B}-1) \right)^{-1/2}$$

otherwise we are in case (ii) and

$$\text{(ii)}: \quad \hat{k} = \frac{1}{2}\left(\frac{\hat{\mathrm{A}}^2}{\hat{\mu}} - 2(\hat{B}-1) \right)^{1/2}.$$

- (parameter q and z) For simplicity, let $s_n = zn + q$. Define $m \in \mathbb{N}$ as the number of segments in which the function u_n is monotone. We counted m manually, although it could also be estimated by, for example,

$$\begin{cases} \text{(i)}: \quad \hat{m} = \left\lceil (N-1)\hat{h}\dfrac{\sqrt{\hat{\mu}}}{K(\hat{k})} \right\rceil (+1), \\ \text{(ii)}: \quad \hat{m} = \left\lceil (N-1)\hat{h}\dfrac{\sqrt{\hat{\mu}}}{2K(\hat{k})} \right\rceil (+1), \end{cases}$$

where K is the complete elliptic integral of the first kind, and the term in brackets $(+1)$ is added only if both u_0 and u_{N-1} are simultaneously increasing or decreasing. Now, using the fact that $\mathrm{sn}^{-1} = F \circ \arcsin$, $\mathrm{cn}^{-1} = F \circ \arccos$, where F is the elliptic integral of the first kind, we can simply invert the Jacobi elliptic function at the endpoints $n = 0$ and $n = N-1$ to obtain q and z. We treat each of the cases (i) and (ii) separately.

(i): From Eqs. (86) and (88), we have the following:

$$\mathrm{dn}(\hat{k}^{-1} s_n; \hat{k}) = \frac{\hat{\mu} u_n + \hat{\mathrm{A}}}{2\hat{k}^{-1}\sqrt{\hat{\mu}}},$$

which can be rewritten as

$$\mathrm{sn}(\hat{k}^{-1} s_n; \hat{k}) = \hat{k}^{-1} \sqrt{1 - \left(\frac{\hat{\mu} u_n + \hat{\mathrm{A}}}{2\hat{k}^{-1}\sqrt{\hat{\mu}}} \right)^2} \equiv U_n.$$

Hence, if u_n is decreasing on the first segment:

$$s_0 = \hat{k} F(\arcsin U_0; \hat{k}),$$

and

$$s_{N-1} = (m-1)\hat{k}K(\hat{k}) + \hat{k}F(\arcsin U_{N-1}; \hat{k}),$$

if m is odd, or

$$s_{N-1} = m\hat{k}K(\hat{k}) - \hat{k}F(\arcsin U_{N-1}; \hat{k}),$$

if m is even. If u_n is increasing on the first segment:

$$s_0 = 2\hat{k}K(\hat{k}) - \hat{k}F(\arcsin U_0; \hat{k}),$$

and

$$s_{N-1} = (m+1)\hat{k}K(\hat{k}) - \hat{k}F(\arcsin U_{N-1}; \hat{k}),$$

if m is odd, or

$$s_{N-1} = m\hat{k}K(\hat{k}) + \hat{k}F(\arcsin U_{N-1}; \hat{k}),$$

if m is even.

(ii): From Eqs. (87) and (88) we have the following:

$$\mathrm{cn}(zn + q; \hat{k}) = \frac{\hat{\mu} u_n + \hat{\mathrm{A}}}{2\hat{k}\sqrt{\hat{\mu}}} \equiv U_n.$$

Hence, if u_n is decreasing on the first segment:

$$s_0 = F(\arccos U_0; \hat{k}),$$

and

$$s_{N-1} = 2(m-1)K(\hat{k}) + F(\arccos U_{N-1}; \hat{k}),$$

if m is odd, or

$$s_{N-1} = 2mK(\hat{k}) - F(\arccos U_{N-1}; \hat{k}),$$

if m is even. If u_n is increasing on the first segment:

$$s_0 = 4K(\hat{k}) - F(\arccos U_0; \hat{k}),$$

and

$$s_{N-1} = 2(m+1)K(\hat{k}) - F(\arccos U_{N-1}; \hat{k}),$$

if m is odd, or

$$s_{N-1} = 2mK(\hat{k}) + F(\arccos U_{N-1}; \hat{k}),$$

if m is even.

Finally, for both cases we set

$$\hat{q} = s_0, \quad \hat{z} = \frac{1}{N-1}(s_{N-1} - s_0).$$

- (parameters x_0 and y_0) From the previous steps, using all the recovered parameters, construct a

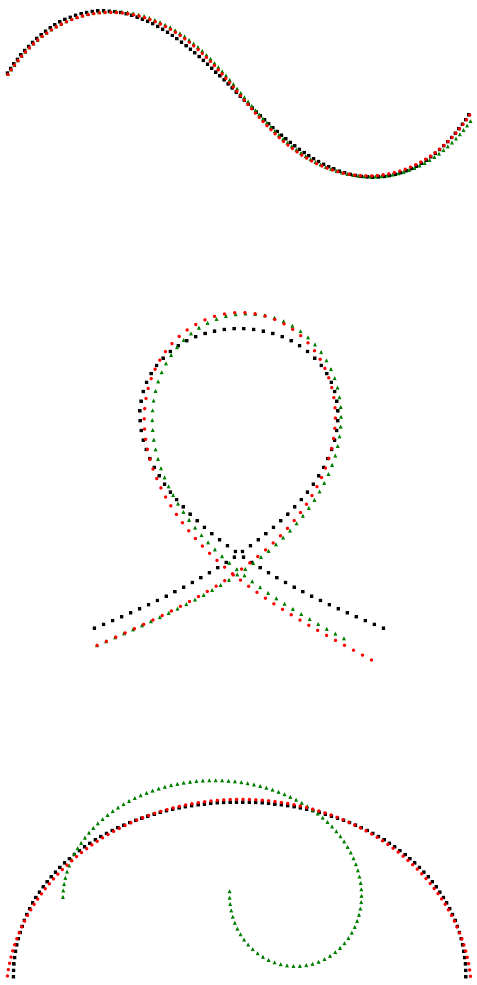

Fig. 6. Typical examples of the fairing by the discrete elasticae. Black squares: input curve, green triangles: initial guess, red circles: output elastica.

discrete elastica segment that starts at the origin, $\gamma_n(\bar{p})$ with $\bar{p} = (0, 0, h, \hat{\phi}, \hat{z}, \hat{q}, \hat{k})$. Then,

$$(\hat{x}_0, \hat{y}_0) = \underset{(x_0,y_0)}{\arg\min} \left\{ \sum_{n=0}^{N-1} (\zeta_n - \gamma_n(\bar{p}))^2 \right\}.$$

Figure 6 illustrates typical examples of the fairing by the discrete elasticae obtained by using the above algorithm.

5. Application: Characterization of Keylines of Japanese Handmade Pantiles

5.1. *Background and outline*

Sangawara (Japanese pantiles) are the most common type of roof tiles in Japan and are thought to

Fig. 7. Beating (top) and stroking (bottom) in making handmade pantiles in demonstration class at Department of Architecture, Mukogawa Women's University.

be unique to the country. Although the number of buildings with sangawara roofs is decreasing, the landscapes with the remaining constructions having sangawara roofs are considered by the community to be one of the most beautiful scenes and culturally Japanese. Traditionally, sangawara were handmade from local clay by placing a clay plate on a wooden mold, beating it with a board called *tataki*, and stroking it with a board called *nadeita* (Fig. 7).

In recent times, they are mass-produced by metal mold presses in limited areas. The mold shapes are thought to be based on the shape of the sangawara in the handmade era, but companies keep their designs a trade secret, so it is not clear. We consider that it is important to characterize esthetically pleasing curves like sangawara with mathematical formulas to be used in architectural design. Because of this, and the fact that the process involves bending the clay plate, we thought that the shape of sangawara could possibly be approximated by elasticae. In Sec. 5.2, we explain how the handmade sangawara (simply referred to as pantiles) were collected, in Sec. 5.3 we obtain the keyline of each pantile, and in Sec. 5.4 we approximate those keylines to discrete elasticae.

5.2. *Data acquisition*

The pantiles we measured had been used in a house built around 1900 in Settsu City, Osaka Prefecture (Fig. 8). From the characteristic shapes of the pantiles, they were likely used from the original construction or replaced before the revision of the urban building law in 1924 after the Great Kanto Earthquake. According to the owners, most of the tiles were blown away when the 2nd Muroto Typhoon hit in 1961, so they were collected and re-roofed. After that, only a few of the pantiles were replaced before the house was demolished in March 2017.

In our survey before the demolition, we found that the roofs of this house were covered by four different sizes of pantiles that ranged from 240 mm to 280 mm in working width. Prior to dismantling the building, we preserved six rows of pantiles (row A to row F in Fig. 9) that covered those four sizes. The pantiles varied in shape due to their handmade nature, so we preserved six rows instead of only four individual pantiles. We measured 37 pantiles from the rows C and F with a working width of 270 mm (the most commonly used on this house), excluding the eave pantiles (pantiles C01 and F01).

Fig. 8. Exterior photos of the house with handmade pantile roof.

The 3D data of each pantile was acquired by using the NextEngine's Ultra HD 3D laser scanner. In Fig. 10, we show a diagram of the setup. The mesh data was then read by the 3D Systems' RapidWorks 64 4.1.0 reverse modeling software. Furthermore, we used this software to synthesize and discard its polygons finer than the scanner's measurement accuracy (0.3 mm) and then automatically launder incorrect data and fill holes in the meshes. For each pantile, we extracted two 3D keylines corresponding to the two front edges that could be observed when pitched. The upper 3D keyline was generated by extracting the curve network from the mesh data, and the lower 3D keyline was generated by extracting the outer boundary curve of the mesh data. In both cases, we used RapidWorks for this process. In Fig. 11, we show an example of the two 3D keylines generated. Finally, we note that each of these 3D keylines are indeed discrete curves in $\mathbb{R}^3$; however, we need to process them to obtain discrete planar curves to be used in the fairing algorithm.

5.3. *Pre-processing*

Projection into discrete planar curves

In order to generate discrete planar curves from the 3D keyline data, we projected the points in $\mathbb{R}^3$ onto the plane which minimizes the sum of the squared distances to the points. As is well known, such plane is constructed by applying the principal component analysis of the so-called covariance matrix. Concretely, let $p_1, p_2, \ldots, p_M \in \mathbb{R}^3$ be the 3D keyline data of one of the edges of one pantile, and define

$$\bar{p} := \frac{1}{M} \sum_{k=1}^{M} p_k. \tag{94}$$

Consider the covariance matrix

$$\mathrm{Cov}[p] := \frac{1}{M} \sum_{k=1}^{M} (p_k - \bar{p})^t (p_k - \bar{p}) \in \mathbb{R}^{3\times 3},$$

which is symmetric and positive semi-definite, and let $e_1, e_2, e_3 \in \mathbb{R}^3$ be orthonormal eigenvectors associated to the eigenvalues $\lambda_1, \lambda_2, \lambda_3 \in \mathbb{R}$ $(\lambda_1 \geq \lambda_2 \geq \lambda_3 \geq 0)$ of $\mathrm{Cov}[p]$. Then, it is known that the plane $\Pi_{12} \subset \mathbb{R}^3$ that includes $\bar{p}$ and is parallel to e_1 and e_2 (i.e., with e_3 as the normal vector) minimizes the sum of the squared distances to $p_1, p_2, \ldots, p_M$ (see, for example, Ref. 29).

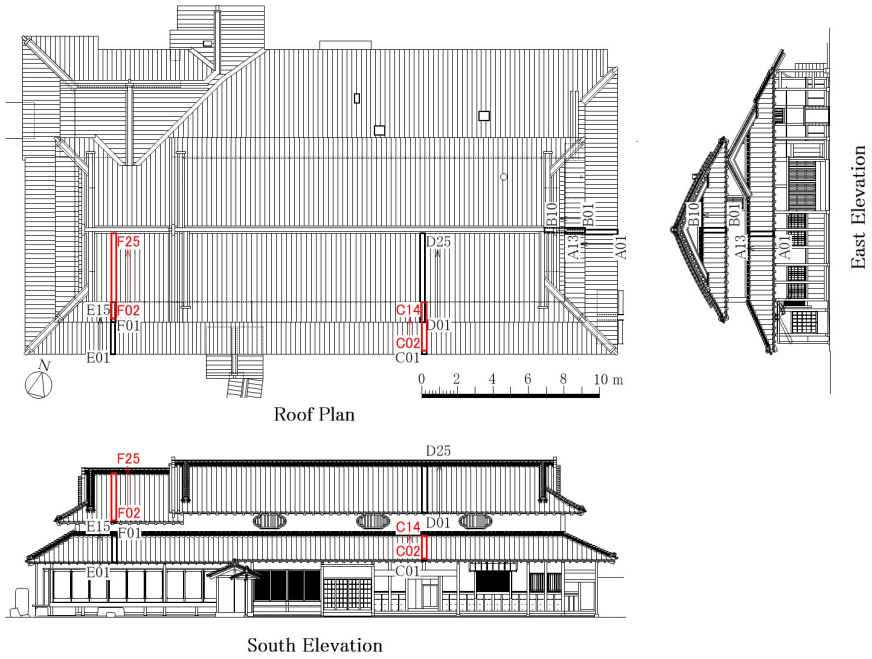

Fig. 9. (Color online) Preserved pantiles (rows A–F) and measured pantiles (in red: pantiles C02–C14, and pantiles F02–F25).

Following this idea, we changed the original xyz-coordinate system into the $x'y'z'$-coordinate system, where $\bar{p}$ is the origin O' and the orientations of e_1, e_2, and e_3 are the x'-, y'-, and z'-axes, respectively, as shown in Fig. 10. The change of coordinates of p_k in the xyz-coordinate system to p'_k in the $x'y'z'$-coordinate system satisfies

$$p'_k = {}^t(e_1\, e_2\, e_3)(p_k - \bar{p}),$$

because $(e_1\, e_2\, e_3)$ is an orthogonal matrix. Finally, the projection of p_k onto Π_{12} was obtained by removing the z'-component from p'_k $(k = 1, \ldots, M)$.

Conversion to constant step sizes

The discrete curves obtained by projecting the 3D keylines onto their corresponding $x'y'$-plane (simply referred to as the 2D keylines before approximation)

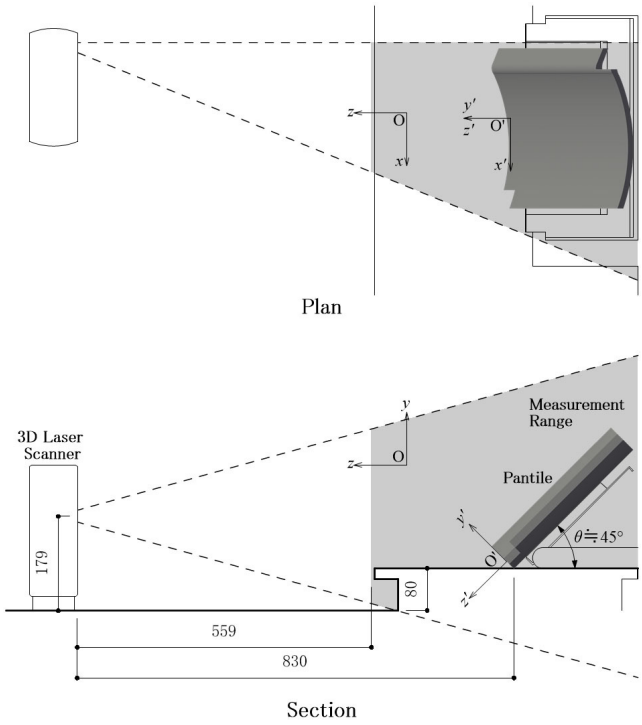

Fig. 10. Placement of the 3D laser scanner and the pantile for measurement.

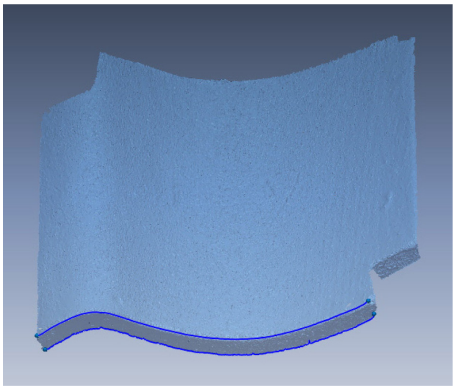

Fig. 11. (Color online) Example of the 3D data acquired for pantile C07. In blue: upper and lower 3D keylines.

do not have constant step sizes. We applied the following procedure to approximate them by constant step-size discrete curves:

(1) Let the leftmost point of the 2D keyline before approximation, on the negative side of the x'-axis, be the starting point A_1.
(2) Let the point on the keyline whose distance from A_1 is r $(= 1.0\,\text{mm})$ be A_2.
(3) For $k = 2, 3, \ldots$, let the point on the keyline whose distance from A_k is r and does not return to A_{k-1} be A_{k+1} (Fig. 12). However, if there are multiple points that satisfy this condition, let the point on the keyline closer to the rightmost point, on the positive side of the x'-axis, be A_{k+1} (Fig. 13).
(4) The final point $k = N$ is set when the only point that has a distance r from A_N is the one that returns to A_{N-1}. A_N is the stop point of the 2D keyline after approximation (Fig. 14).

Note that the resulting curve $A_k \in \mathbb{R}^2$, $k = 1, \ldots, N$, is a discrete planar curve with constant step size r.

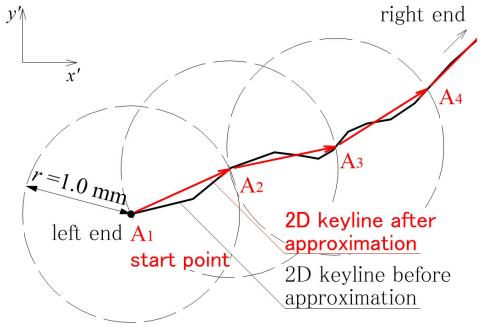

Fig. 12. Procedure to construct a constant step-size discrete planar curve (pantile C07, lower keyline).

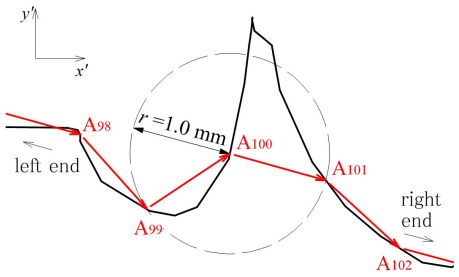

Fig. 13. Visualization of the method for determining the following point when there are multiple points whose distance is r (pantile C07, lower keyline).

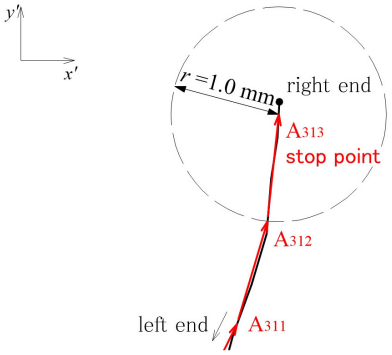

Fig. 14. Visualization of the method for determining the stop point (pantile C07, lower keyline).

Principal axis alignment

When measuring the pantiles as shown in Fig. 10, we placed them one by one on the table by hand. Therefore, the position and rotation angle of each pantile is slightly different. To compare the shapes of the keylines of the measured pantiles, we have to eliminate the effects of the positions and rotation angles and convert them into a coordinate system determined by only the keyline shape. This effect was eliminated by changing the coordinates and projecting them from the xyz-coordinate system into the $x'y'$-coordinate system, where the geometric center is O', the orientation of its first principal component is the x'-axis, and the orientation of its second principal component is the y'-axis. However, this alignment is lost after approximating the discrete curves to constant step-size discrete curves. Hence, we performed a principal component analysis again, but on the plane containing the discrete curve A_k, $k = 1, \ldots, N$. Let

$$\bar{\mathrm{A}} = \frac{1}{N}\sum_{k=1}^{N} A_k,$$

and f_1, f_2 be normalized eigenvectors that correspond to the eigenvalues μ_1, μ_2 $(\mu_1 \geq \mu_2)$ of the covariance matrix

$$\mathrm{Cov}[A] = \frac{1}{N}\sum_{k=1}^{N}(A_k - \bar{\mathrm{A}})^t(A_k - \bar{\mathrm{A}}) \in \mathbb{R}^{2\times 2}.$$

Here, the directions of f_1 and f_2 are determined so that the diagonal components of $(f_1\, f_2)$ are all positive. Then, the $x'y'$-coordinate system is transformed to the $x''y''$-coordinate system, where $\bar{\mathrm{A}}$ as the origin O'' and x'' as the first principal axis (in the direction of f_1). Finally, we denote to as A'_k

$(k = 1, \ldots, N)$ to the discrete curve in the new coordinate system, which satisfies that

$$A'_k = {}^t(f_1\, f_2)(A_k - \bar{\mathrm{A}}),$$

because $(f_1\, f_2)$ is an orthogonal matrix. In what follows, the $x''y''$-coordinate system is redefined as the xy-coordinate system.

Estimation of inflection points

If we visualize and smooth curve fairing the 2D keyline of the pantile, it has one global inflection point and its shape is clearly asymmetric across the inflection point. In general, it is difficult to formulate such a curve in terms of a single elastica. Therefore, we estimated the global inflection point of the approximate curve, then we divided the curve on both sides of the inflection point and fair them with two different elastic curves. We estimated the inflection point using a method inspired by the Ramer–Douglas–Peucker (RDP) algorithm,[30,31] which was devised to simplify an open polygon with many vertices by thinning out some of the vertices (Fig. 15). We call this the RDP method:

(1) Let the point farthest from the line segment connecting the two end points be 3. Let the end point on the side with the inflection point (viewed from point 3) be 2, and let the end point on the side without the inflection point be 1.

(2) For $P = 2, 3, \ldots$, among the points of the discrete curve between P and $P+1$, let the point farthest from the line segment $P(P+1)$ be $P+2$. However, the labels of P and $P+1$ are switched if one of the next two conditions hold:

   (a) $P+1$ is in the upper side of the line segment $(P-1)P$ and point $P+2$ is in the upper side of the line segment $P(P+1)$.

   (b) $P+1$ is in the lower side of the line segment $(P-1)P$ and point $P+2$ is in the lower side of the line segment $P(P+1)$.

(3) The computation is terminated when there is no more points between $P+1$ and $P+2$, and the inflection point is estimated to be $P+2$.

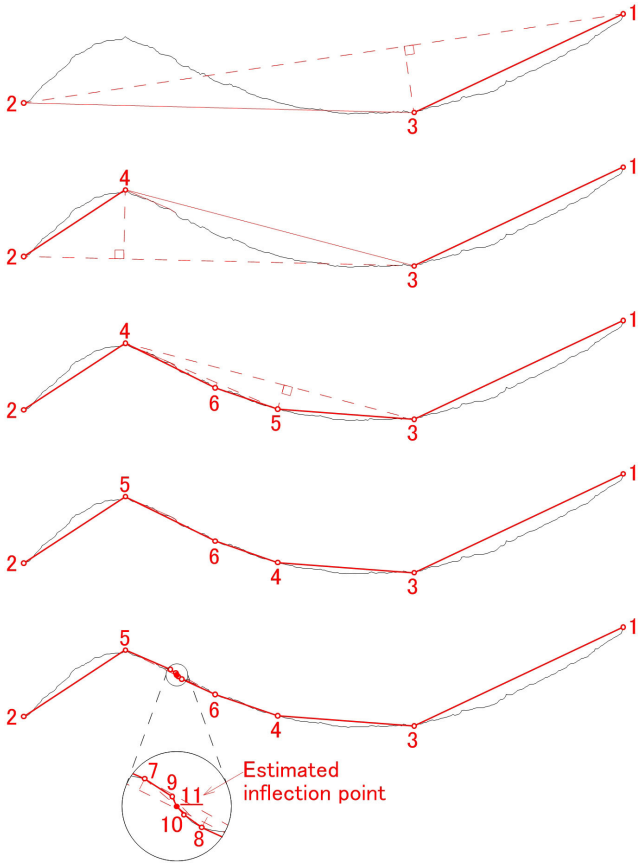

Fig. 15. Example of inflection point estimation by the RDP method (pantile C07, lower keyline). From top to bottom, the first curve represents step (1). The second and third curves represent step (2). The fourth curve shows the particular case when switching the labels 4 and 5 is needed for case (2-b). The fifth and last curve represents the termination condition of step (3), where the inflection point is estimated to be at the point 11.

5.4. *Approximation by discrete Euler's elasticae*

We considered the 37 lower keyline segments situated at the right-hand side of the inflection point (i.e., the valley portion of the keylines), see Fig. 16. For each discrete planar curve we applied the fairing algorithm as described in Sec. 4. Among the parameters $p = (x_0, y_0, h, \phi, z, q, k)$ shown in Eq. (71), the point (x_0, y_0) was set at the inflection

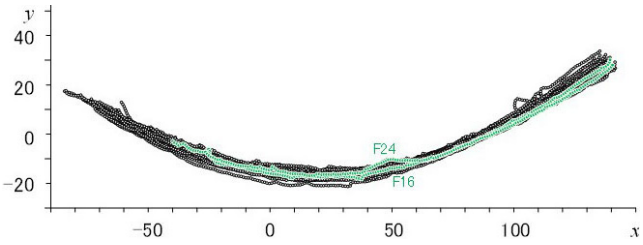

Fig. 16. Input curves: Right (valley) sides of the 2D lower keylines corresponding to pantiles C02–C14 and pantiles F02–F25. The highlighted curves (pantiles F16 and F24) presented statistically different results.

Table 1. Calculation results for h, ϕ, z, q and k (mean and standard deviation).

Lower keylines right (valley) side		h [mm]	ϕ [rad]	ϕ [grad]	z	q	k
C02–14, F02–15, 17–23, 25	[mean]	0.964	−0.168	−9.623	9.001×10^{-3}	5.919	0.353
	[std. dev.]	6.564×10^{-3}	2.078×10^{-3}	0.119	1.263×10^{-3}	1.789×10^{-3}	1.235×10^{-2}
F16		0.945	2.045	117.192	67.36	5.226	27.43
F24		1.007	2.478	141.986	121.8	28.28	27.39

Notes: Because the values for pantiles F16 and F24 were very different from the others, the means and standard deviations were calculated for the 35 keylines except for pantiles F16 and F24, and the values for them were written separately.

point and the remaining five parameters were optimized. An example of the approximation of a keyline (pantile C07, lower keyline) by a discrete elastica is shown in Fig. 17, the calculation results for the 37 fairing discrete elasticae are shown in Fig. 18, and the calculation results for the parameters h, ϕ, z, q, k are shown in Table 1.

As Table 1 shows, the 35 key lines (except for pantiles F16 and F24) show very little variation in the calculated results of the parameters, and the discrete elasticae are similar in both shape and rotation angle. The k values are close to 0.3, and the shapes are close to sine curves. However, the values of ϕ, z, q, and k for pantiles F16 and F24 are very different from the others. The k values exceed 10, and the shapes are close to arcs.

Figure 19 shows the 37 translated discrete elasticae shown in Fig. 18 with the inflection point (x_0, y_0) at the origin. The variations of the discrete elasticae are larger than that in Fig. 18, suggesting that a certain number of variations and errors may be included in the estimations of the inflection points. In F16 and F24 in particular, the estimated inflection points are located closer to the right (valley) sides. Therefore, we can assume that the areas around the inflection points where the curvature is small are largely omitted, and the discrete elasticae are approximated to be close to the arcs. The effect the local unevenness of the keyline has on the estimation of the inflection point should be examined.

In conclusion, we found that 35 of the 37 lower keylines of the handmade pantiles could be approximated by discrete elasticae with a very small variation on the right (valley) side of the inflection point. However, the errors of the estimated positions of the inflection points may affect the accuracy of the approximations.

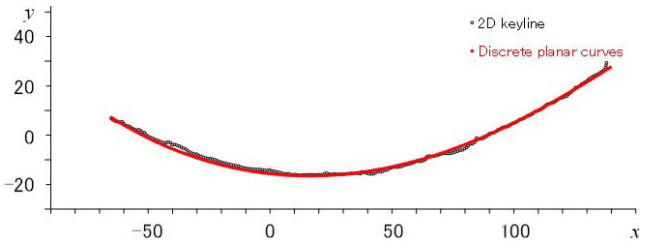

Fig. 17. (Color online) Example: fairing of the pantile C07 lower keyline (black) to a discrete elastica (red).

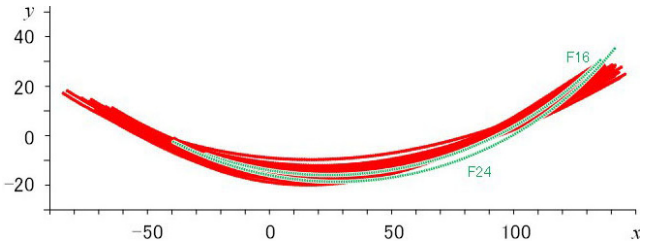

Fig. 18. Output curves: fairing discrete elasticae. The highlighted curves presented statistically different results.

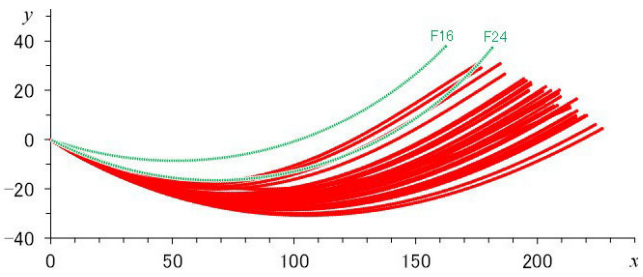

Fig. 19. Result of translating the discrete elasticae in Fig. 18 so that each inflection point is at origin. Calculation results of F16 and F24 are clearly different from the others.

Acknowledgments

The authors would like to thank Professor David Brander for encouragement. They also express their thanks to Professors Nozomu Matsuura, Jun-ichi Inoguchi, Kenjiro T. Miura, Satoshi Kanai and Dr. Masahisa Asada for fruitful discussions. They would like to thank Mr. Konosuke Onishi, Mr. Yunosuke Onishi, Associate Professor Toshikazu Inoue, and Mr. Daisuke Mitsumoto for their cooperation in the housing survey. This work was initiated by the 2018 IMI Joint Use Research Program Short-Term Joint Research No. 20180008, and supported by JSPS Kakenhi Nos. JP16H03941, 17K00741, 20K12520, 21K03329 and JST CREST Grant No. JPMJCR1911.

References

1. S. Matsutani, Euler's elastica and beyond, *J. Geom. Symmetry Phys.* **17** (2010) 45–86, doi: 10.7546/jgsp-17-2010-45-86.
2. D. A. Singer, Lectures on elastic curves and rods, in *Curvature and Variational Modeling in Physics and Biophysics*, Vol. 1002. (American Institute of Physics Conference Series, 2008), pp. 3–32.
3. D. Brander, J. Gravesen and T. B. Nørbjerg, Approximation by planar elastic curves, *Adv. Comput. Math.* **43** (2017) 25–43.
4. A. I. Bobenko and Y. B. Suris, Discrete time Lagrangian mechanics on lie groups, with an application to the Lagrange top, *Commun. Math. Phys.* **204** (1999) 147–188.
5. NIST digital library of mathematical functions, https://dlmf.nist.gov/.
6. R. E. Goldstein and D. M. Petrich, The Korteweg-De Vries hierarchy as dynamics of closed curves in the plane, *Phys. Rev. Lett.* **67** (1991) 3203–3206.
7. J. Inoguchi, K. Kajiwara, N. Matsuura and Y. Ohta, Motion and Bäcklund transformations of discrete planar curves, *Kyushu J. Math.* **66** (2012) 303–324.
8. D. F. Lawden, *Elliptic Functions and Applications*, Applied Mathematical Sciences, Vol. 80. (Springer-Verlag, New York, 1989).
9. T. Hoffmann, *Discrete Differential Geometry of Curves and Surfaces*, IMI Lecture Notes, Vol. 18. (Kyushu University, Fukuoka, 2009).
10. J. Inoguchi, K. Kajiwara, N. Matsuura and Y. Ohta, Discrete mKdV and discrete sine-Gordon flows on discrete space curves, *J. Phys. A, Math. Theoret.* **47**(23) (2014) 235202.
11. N. Matsuura, Discrete KdV and discrete modified KdV equations arising from motions of planar discrete curves, *Int. Math. Res. Notices* **2012**(8) (2012) 1681–1698, doi: 10.1093/imrn/rnr080.
12. A. I. Bobenko, Geometry II — Discrete differential geometry (2020), https://page.math.tu-berlin.de/~techter/lecture_notes/geometry2-ddg.pdf.
13. T. Hoffmann and N. Kutz, Discrete curves in $\mathbb{C}p^1$ and the Toda lattice, *Stud. Appl. Math.* **113** (2004) 31–55.
14. D. Takahashi, T. Tokihiro, B. Grammaticos, Y. Ohta and A. Ramani, Constructing solutions to the ultradiscrete painlevé equations, *J. Phys. A, Math. Gen.* **30** (1997) 7953–7966.
15. G. R. W. Quispel, J. A. G. Roberts and C. Thompson, Integrable mappings and soliton equations, *Phys. Lett. A* **126** (1988) 419–421.
16. K. Kajiwara, Y. Ohta, J. Satsuma, B. Grammaticos and A. Ramani, Casorati determinant solutions for the discrete painlevé-ii equation, *J. Phys. A, Math. Gen.* **27** (1994) 915–922.
17. K. Kajiwara, M. Noumi and Y. Yamada, Geometric aspects of painlevé equations, *J. Phys. A, Math. Theor.* **50** (2017) 073001.
18. A. Ramani, B. Grammaticos and J. Hietarinta, Discrete versions of the painlevé equations, *Phys. Rev. Lett.* **67** (1991) 1829–1832.
19. N. Matsuura, An explicit formula for discrete planar elastic curves, talk given at the Annual Meeting of Mathematical Society of Japan (2020), (in Japanese).
20. D. Mumford, Elastica and computer vision, in *Algebraic Geometry and Its Applications* (Springer, New York, 1994), pp. 491–506.
21. K. Sogo, Variational discretization of Euler's elastica problem, *J. Phys. Soc. Jpn.* **75** (2006) 064007.
22. A. Bobenko and U. Pinkall, Discrete surface with constant negative Gaussian curvature and the Hirota equation, *J. Differential Geom.* **43** (1996) 527–611.
23. R. Hirota, Nonlinear partial difference equations. III. Discrete sine-Gordon equation, *J. Phys. Soc. Jpn.* **43** (1977) 2079–2086.
24. R. Hirota, Discretization of the potential modified KdV equation, *J. Phys. Soc. Jpn.* **67** (1998) 2234–2236.
25. J. Fernández, S. E. Graiff Zurita and S. Grillo, Error analysis of forced discrete mechanical systems, *J. Geom. Mech.* (2021), doi: 10.3934/jgm.2021017.
26. J. E. Marsden and T. S. Ratiu, *Introduction to Mechanics and Symmetry*, Texts in Applied Mathematics, Vol. 17, 2nd edn. (Springer-Verlag, New York, 1999).
27. G. W. Patrick and C. Cuell, Error analysis of variational integrators of unconstrained Lagrangian systems, *Numer. Math.* **113** (2009) 243–264.

28. A. Wächter and L. Biegler, On the implementation of an interior-point filter line-search algorithm for large-scale nonlinear programming, *Math. Program., Ser. A* **106** (2006) 25–57.
29. J. Berkmann and T. Caelli, Computation of surface geometry and segmentation using covariance techniques, *IEEE Trans. Pattern Anal. Mach. Intell.* **16** (1994) 1114–1116.
30. D. Douglas and T. Peucker, Algorithms for the reduction of the number of points required to represent a digitized line or its caricature, *Cartographer* **10** (1973) 112–122.
31. U. Ramer, An iterative procedure for the polygonal approximation of plane curves, *Comput. Graph. Image Process.* **1** (1972) 244–256.